

Konrad, K., Jackson, M., Steinberger, B., Koppers, A., Balbas, A., Finlayson, V., Konter, J., Price, A. (2024): Toroidal flow around the Tonga slab moved the Samoan plume during the Pliocene. - *Geology*, 52, 3, 176-180.

<https://doi.org/10.1130/G51588.1>

1 **Toroidal Flow Around the Tonga Slab Moved the Samoan Plume During the**  
2 **Pliocene**

3  
4 Kevin Konrad<sup>1</sup>; Matthew Jackson<sup>2</sup>; Bernhard Steinberger<sup>3</sup>; Anthony Koppers<sup>4</sup>; Andrea Balbas<sup>5</sup>;  
5 Valerie Finlayson<sup>6</sup>; Jasper Konter<sup>7+</sup>; Allison Price<sup>8</sup>

6  
7 1. Department of Geoscience, University of Nevada Las Vegas, Las Vegas, Nevada 89154, USA

8 2. Department of Earth Science, University of California Santa Barbara, California 93106, USA

9 3. GFZ German Research Centre for Geosciences, Telegrafenberg, 14473 Potsdam, Germany

10 4. College of Earth, Ocean and Atmospheric Sciences, Oregon State University, Corvallis,

11 Oregon 97331 USA

12 5. Department of Geological Sciences, California State University Long Beach, Long Beach, CA

13 90840, USA

14 6. Department of Geology, University of Maryland College Park, College Park, Maryland 20742

15 7. Department of Earth Sciences, School of Ocean and Earth Science and Technology,

16 University of Hawai‘i Mānoa, Honolulu, Hawaii 96822 USA

17 8. Los Alamos National Laboratory, Los Alamos, New Mexico, USA, 87545, USA

18

## 19 **ABSTRACT**

20 Age-progressive seamount tracks generated by lithospheric motion over a stationary  
21 mantle plume have long been used to reconstruct absolute plate motion (APM) models.  
22 However, the basis of these models require the plumes be fixed relative to the overriding  
23 lithosphere. When a plume interacts with a convergent or divergent boundary, it is often  
24 deflected within the strong local mantle flow fields associated with such regimes. Here we  
25 examine the age progressions and geometry of the Samoa hotspot track focusing on lava flow  
26 samples dredged from the deep flanks of the seamounts in order to best reconstruct when a given  
27 seamount was overlying the mantle plume (e.g., during the shield building stage). The Samoan  
28 seamounts display an apparent local plate velocity of 7.8 cm/a from 0 – 9 Ma, 11.1 cm/a from 9-  
29 14 Ma and 5.6 cm/a from 14-24 Ma. Current fixed- and mobile-hotspot Pacific APM models  
30 cannot reproduce the geometry of the Samoa seamount track if a long-term fixed hotspot  
31 location, currently beneath the active Vailulu’u seamount, is assumed. Rather, reconstructing the  
32 eruptive locations of the Samoa seamounts using APM models indicates that the surface  
33 expression of the plume migrated  $\sim 2^\circ$  northward in the Pliocene. Large-scale mantle flow in the  
34 Pacific cannot explain the plume migration. Instead, the best fit explanation is that toroidal flow  
35 fields—generated by westward migration of the Tonga Trench and associated slab rollback—  
36 have deflected the conduit northward over the last 3-2 Ma. These observations provide novel  
37 constraints on how plume-trench interaction can alter hotspot track geometries.

## 38 **INTRODUCTION**

39 Age-progressive volcanic chains at hotspots are produced as Earth’s lithosphere migrates  
40 over stationary or slowly moving (relative to plate motions) mantle plumes ([Morgan et al., 1972](#);  
41 [Wessel and Kroenke, 2008](#); [Koppers et al., 2021](#)). This phenomenon provides an ideal natural  
42 constraint to calibrate the motion of lithospheric plates through time relative to a fixed reference  
43 frame, known as an absolute plate motion (APM) model (e.g. [Duncan and Clague, 1985](#); [Wessel](#)  
44 [and Kroenke, 2008](#); [Dobrovine et al., 2012](#)). Utilizing hotspot tracks to produce APM models  
45 requires that any independent motion of the underlying mantle plume is significantly slower,  
46 relative to the motion of the overriding lithosphere ([Wessel and Kroenke, 2008](#)). To a first order,  
47 this assumption appears to be validated by APM models reproducing the geometry and age-  
48 progressions of numerous seamount chains on the same plate ([Duncan and Clague, 1985](#); [Wessel](#)

49 and Kroenke, 2008; Konter et al., 2023). Numerical models of plume ascent in mantle flow fields  
50 predict that plumes should move independently through time as a function of deflection in  
51 mantle convective fields, however precisely predicting movements requires accurate knowledge  
52 of the plume's viscosity, buoyancy, and size relative to the ambient mantle (Steinberger, 2000;  
53 Doubrovine et al., 2012; Konrad et al., 2018). Thus, independent observations of potential plume  
54 movement are required to test and constrain models (e.g. Tarduno et al., 2003; Koppers et al.,  
55 2012; Konrad et al., 2018).

56 To date, the only plume that has shown significant evidence (i.e., via age-progressions,  
57 paleomagnetic reconstructions and numerical models) of rapid independent motion in the Pacific  
58 basin is the Hawaiian-Emperor plume in the 80-50 Ma timeframe (Tarduno et al., 2003; Wessel  
59 and Kroenke, 2009; Konrad et al., 2018). However, others have argued that motions between  
60 Pacific plumes are not required to fit the observed inter-hotspot distance trends, and the age-  
61 progressions are biased by minimal seamount sampling in the Emperor seamount chain and true  
62 polar wander occurring in the Eocene-Cretaceous, explaining the paleomagnetic observations  
63 (Gaastra et al., 2022). In addition, independent tests of mobile versus fixed hotspot APM models  
64 have indicated that the fixed hotspot model better fits Pacific hotspot track age-progressions and  
65 geometry (Wang et al., 2019). Here we compile age determinations for lava flows sourced by the  
66 Samoan plume to provide evidence that the apparent surface expression of the hotspot has not  
67 been fixed, but instead has shifted northward by 2° during the Pliocene. Shallow mantle flow  
68 resulting from the approaching Tonga trench is likely responsible for the shift. This provides  
69 novel insights into the role plate-plume interaction plays in affecting apparent age-progressions  
70 and geometry of seamount chains.

## 71 THE SAMOAN SEAMOUNT PROVINCE

72 The Samoan plume has been sourcing islands and seamounts since at least 24 Ma  
73 (Duncan 1985; Hart et al., 2004; Koppers et al., 2011; **Fig. 1**). The Samoan hotspot track consists  
74 of active and recent volcanism on the eastern end beneath Vailulu'u and Malumalu seamounts  
75 (Hart et al. 2000; Sims et al., 2008; Koppers et al., 2011) and extends westward to *ca.* 24 Ma  
76 volcanism on Alexa Bank on the westernmost end (Hart et al., 2004). Complicating the age-  
77 progressions and geomorphology of the seamount chain are pulses of non-Samoan plume related  
78 volcanism, including ancient structures likely related to the Ontong-Java Nui large igneous  
79 province (Robbie Ridge; Chandler et al., 2012; **Fig. 1**), Eocene seamounts sourced from the

80 Rurutu-Arago hotspot (Konrad et al., 2018; Finlayson et al., 2018), and recent small-scale,  
81 sporadic petite spot-like volcanism likely related to the advancement of the Tonga Trench over  
82 the last ~5 Ma (Hart et al., 2004; Sims et al., 2008; Strak and Schellart, 2018; Reinhard et al.,  
83 2019; Price et al., 2022). To aid in filtering the noise from this complex region, we define  
84 whether a recovered lava flow is Samoan in origin based on its (or same dredge) isotopic  
85 characteristics (e.g. elevated  $^{87}\text{Sr}/^{86}\text{Sr} > 0.7035$  that is diagnostic of the Samoan Plume; see  
86 compositional fields in Price et al., 2022) as well as following an age-progression consistent with  
87 the Samoan plume (Hart et al., 2004; Koppers et al., 2011). Furthermore, in order to best  
88 estimate when a seamount was directly above the plume, only lava flows dredged from the deep  
89 flanks of islands seamounts (i.e., subaerial lavas are excluded) are employed (Table S1). This is  
90 done to best represent the time of the shield building stage (e.g. Koppers et al., 2008) as well as  
91 to avoid biasing the data towards heavily sampled structures. The lava flows used in this study  
92 are listed in the **Table S1** and shown in **Fig. 2**.

### 93 **Age Progressions**

94 Previous work on local plate velocity constraints using age progressions of Samoan  
95 volcanoes were complicated by significant rejuvenated volcanism on the islands (e.g. Workman  
96 et al., 2004) as well as sporadic reactivation of volcanism throughout the chain due to the  
97 advancement of the Tonga ± Vitiāz Trench (Strak and Schellart, 2018; Reinhard et al., 2019).  
98 **Fig. 2** shows the apparent plate velocity using currently available age constraints for the Samoa  
99 plume sourced seamounts. There are three clear changes in local plate velocity with slopes of 0.7  
100 °/Ma (7.8 cm/a) for 0 – 9 Ma; 1.0°/Ma (11.1 cm/a) for 9-14 Ma and ~0.5°/Ma (5.6 cm/a) for 14-  
101 24 Ma. The mean local velocity for the 0-24 Ma Samoa chain is 0.71°/Ma (7.9 cm/a; **Fig. 2**),  
102 which is similar to previous estimates of ~7.6 cm/a (Koppers et al., 2011). The new local plate  
103 velocity is however slower than what is expected from Pacific APM models calculated without  
104 independent Samoa plume motion (Wessel and Kroenke, 2008: 9.3 cm/a; Doubrovine et al.,  
105 2012: 8.3 cm/a). This slower apparent plate velocity can be explained if the plume is migrating in  
106 a direction with a component of motion in the same direction as plate motion.

### 107 **APPARENT MOTION OF THE SAMOA PLUME**

108  
109 Despite having a consistent age progression from 24 to 0 Ma, the Samoan hotspot track has  
110 been previously shown to contain a geometry that is similar to, but deviated from, Pacific APM-

111 derived model projections of the hotspot track (Brocher et al., 1985; Hart et al., 2004; Koppers et  
112 al., 2008, 2011) (**Fig. 3**). Hart et al. (2004) postulated that the misfit is related to a recent (e.g.  
113 last ~2 or 1 Ma) northward shift of the Samoa hotspot location. Here, we reexamine the evidence  
114 for plume motion using a larger seamount dataset to better constrain if and when the surface  
115 expression of the Samoa plume shifted.

116 To illustrate the apparent plume motion, here we take a set of seamount data (latitude,  
117 longitude, age) and rotate them based on APM models (both fixed and mobile hotspot)  
118 backwards in time to the latitude and longitude where the lava flow initially erupted (e.g., Wessel  
119 and Kroenke, 1997). If the hotspot has remained largely stationary over time, seamounts  
120 comprising a hotspot track will cluster around the active hotspot location. By contrast, plume  
121 motion and/or prolonged late-stage activity at a seamount will result in reconstructions further  
122 away from the modern hotspot. This technique is thus valuable for studies on mantle plume  
123 dynamics to evaluate how plumes have moved relative to the overriding plate. **Figs. 3A and 3C**,  
124 show the reconstructed eruptive locations using the stationary hotspot APM model of Wessel and  
125 Kroenke (2008) (WK08-G) and the mobile hotspot APM model of Doubrovine et al. (2012)  
126 (D12). Both results indicate that the plume was either relatively stationary, or moved non-  
127 systematically within a limited distance (yellow ellipse; **Fig. 3**), from 3 to 15 Ma (mean apparent  
128 hotspot location: WK08 = 16.5°S, 168.7°W; D12 = 15.9°S, 169.2°W). Assuming the main melt  
129 production zone of the plume is currently underlying the active Vailulu'u seamount (14.2°S,  
130 169.05°W; Hart et al., 2000), this result yields a ~2.3° (WK08-G) or 1.7° (D12) shift in the  
131 surface expression between 3 Ma and today. Note that D12 is smoothed to 10 Ma increments but  
132 provides the same first-order observations as the more detailed WK08-G model. To further  
133 illustrate this observation, **Figs. 4B and 4D** show reconstructed hotspot tracks rooted relative to  
134 the current hotspot location (blue star) and the mean 3-15 Ma hotspot location (yellow star). In  
135 both APM models, WK08-G and D12, the adjusted hotspot locations produce a much better fit to  
136 the positions and ages of the >3 Ma Samoa seamounts – indicating the shift in hotspot location  
137 was relatively recent. The <3 Ma Samoa seamounts also display clear *en echelon* structures that  
138 step to the NE instead of a consistent seamount chain that progresses towards the southeast – like  
139 the Hawaiian Islands (Hart et al., 2004; Koppers et al., 2011; **Fig. 1**). This stepwise *en echelon*  
140 structure may be a function of the apparent rapid northward plume motion. What is certain is that  
141 the surface expression of the Samoa plume shifted northward during the Pliocene.

142 What is currently uncertain is whether the plume was located significantly further south  
143 during the emplacement of Alexa Bank at 24 Ma, which has an apparent reconstructed eruptive  
144 location of 18.5°S, 165.8°W (WK08-G). This apparent location is 5.3° SE of Vailulu'u seamount  
145 and ~3.4° SE of the mean 3-15 Ma hotspot location, indicating there was significant  
146 northwestward motion of the plume between 24 Ma and 15 Ma. Unlike the Tonga slab's  
147 approach to the Samoan plume during the Pliocene (discussed below), there are no clear tectonic  
148 drivers for a 3.4° northwestward shift in the plume location between 24-15 Ma apparent at this  
149 time. The eruptive location offset between Alexa and other Samoa seamounts is likely not due to  
150 sampling bias. For instance, if the lava flows dated in [Hart et al. \(2004\)](#) represented late stage or  
151 post-erosional volcanism, then the apparent hotspot location — represented by hypothetical  
152 shield-stage lavas that would be even older — would move further south. In other words, an  
153 emplacement age of *ca.* 17-18 Ma is required for Alexa Bank to 'hotspot' to the same location as  
154 the other 3-15 Ma volcanoes. Therefore, either a plume motion or tectonic model is required to  
155 explain the apparent migration of the Samoa hotspot.

#### 156 **Could Large Scale Mantle Flow be Responsible?**

157 A plume conduit ascending in convecting mantle flow fields should naturally be laterally  
158 advected assuming a reasonable buoyancy flux. Models of mantle flow fields inferred from  
159 seismic tomography derived density differences indicate that the Samoa plume should be  
160 migrating eastward over at least the last 24 Ma ([Steinberger 2000](#); [Hart et al., 2004](#); **Fig. S2, S3**).  
161 In these models, the plume conduit first becomes tilted, with its base moving eastward towards a  
162 large-scale upwelling beneath the central Pacific, whereas its top part moves W to NW-ward  
163 with the flow in the upper part of the mantle driven by Pacific plate motion and subducted slabs.  
164 However, for most plume models using a current hotspot location at Vailulu'u, a straightening up  
165 of the conduit, corresponding to E- to ESE-ward hotspot motion in "recent" times (e.g. since  
166 ~16.6 Ma in Fig. 10 of [Hart et al., 2004](#); since ~30 Ma in **Fig. S2**) is predicted. The model used  
167 in [Hart et al. \(2004\)](#) can potentially explain the northwestward drift in hotspot location between  
168 Alexa (24 Ma) and ~17 Ma. However, in order for the 24-17 Ma time period to still be in the  
169 initial phase, before hotspot motion becomes east- to eastsoutheastward, that model requires the  
170 Samoa plume initiated around 40 Ma or even later, which is inconsistent with evidence for >100  
171 Ma formation of the plume ([Konter et al., 2023](#)). Further sampling of presumed 24-15 Ma  
172 seamounts west of Bayonnaise (**Fig. 1**) is required to test if the plume has migrated

173 northwestward during the early Miocene or if the ages from Alexa Bank are anomalous.  
174 Importantly, none of the seismic tomography-based plume motion models can match the  
175 observed rapid northward migration of the plume over the Pliocene. It is important to note that  
176 the plume motion models (e.g. Steinberger, 2000) are resolved to spherical harmonic degree 63,  
177 which is likely not fine-scale enough to detect smaller, regional asthenosphere flow regimes  
178 related to the Tonga Trench. However, based on current model observations large-scale mantle  
179 flow regimes are likely not responsible for the observed drift.

#### 180 **Could Advancement of the Tonga Trench be Responsible?**

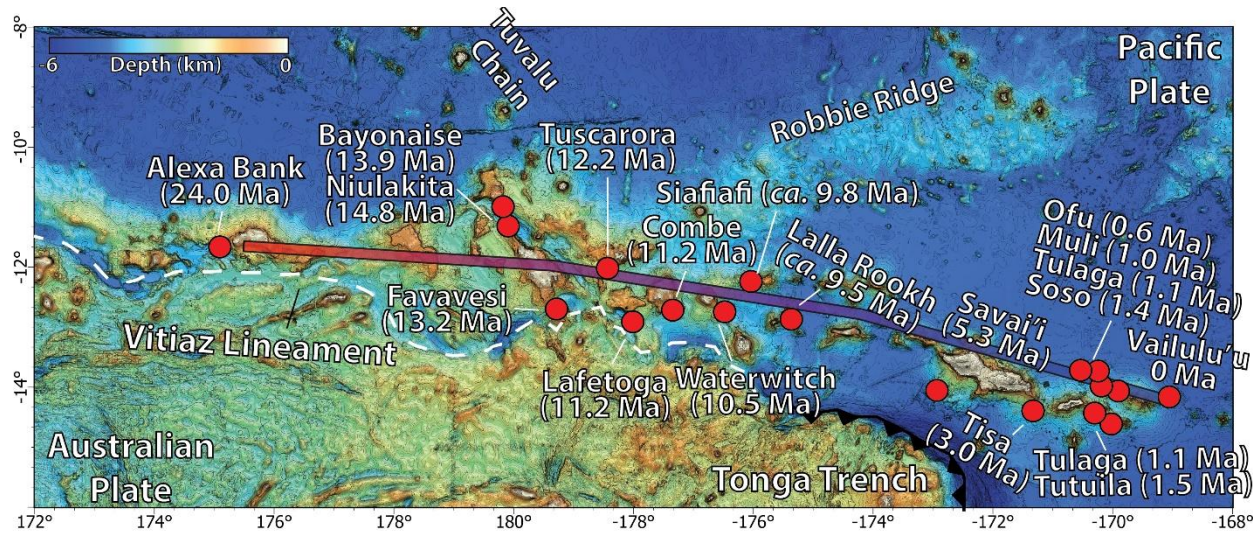
181 The Tonga Trench has been advancing eastward, consuming Pacific lithosphere, over the last  
182 5 Ma (Ruellan et al., 2003). Importantly, the trench has advanced close to the Samoa plume over  
183 the last 2-3 Ma (Hart et al., 2004; Koppers et al., 2008). The rollback of the subducted Pacific  
184 slab is modeled to generate a counterclockwise toroidal mantle flow field in the region of the  
185 Samoan plume today (Strak and Schellart, 2018). This mantle flow field provides a geographic  
186 and temporal fit to the observed sudden Pliocene shift in the surface expression of the Samoan  
187 plume. **Fig. 4** shows a schematic illustration of how the progressing Tonga Trench and  
188 associated rollback can generate toroidal flow fields that deflect the Samoan plume northward.  
189 Prior to 3 Ma, the trench was located too far west of the plume to impact the plume conduit (**Fig.**  
190 **4**). By 3-2 Ma the trench, and associated local mantle flow fields around the Tonga slab, were  
191 proximal enough to deflect the Samoan plume northward, generating an apparent migration of  
192 the plume. Thus, plume-proximal trench interaction can alter the apparent surface expression of  
193 the plume and generate track geometries that are inconsistent with APM models.

194

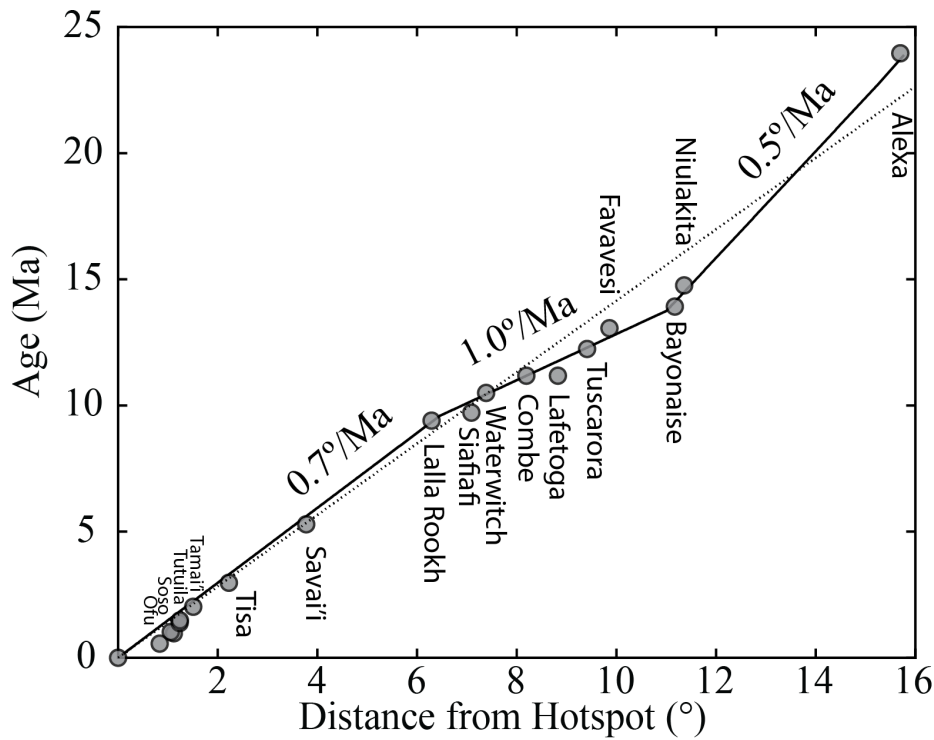
#### 195 **ACKNOWLEDGEMENTS**

196 This study was funded by NSF OCE# 1154070 to AAPK, NSF-OCE #1153894 and #1912931 to  
197 MGJ. BS was supported by the innovation pool of the Helmholtz Association through the  
198 Advanced Earth System Modelling Capacity (ESM) activity. We thank R.G. Gordon, H.P.  
199 Bunge and an anonymous reviewer for their helpful suggestions.



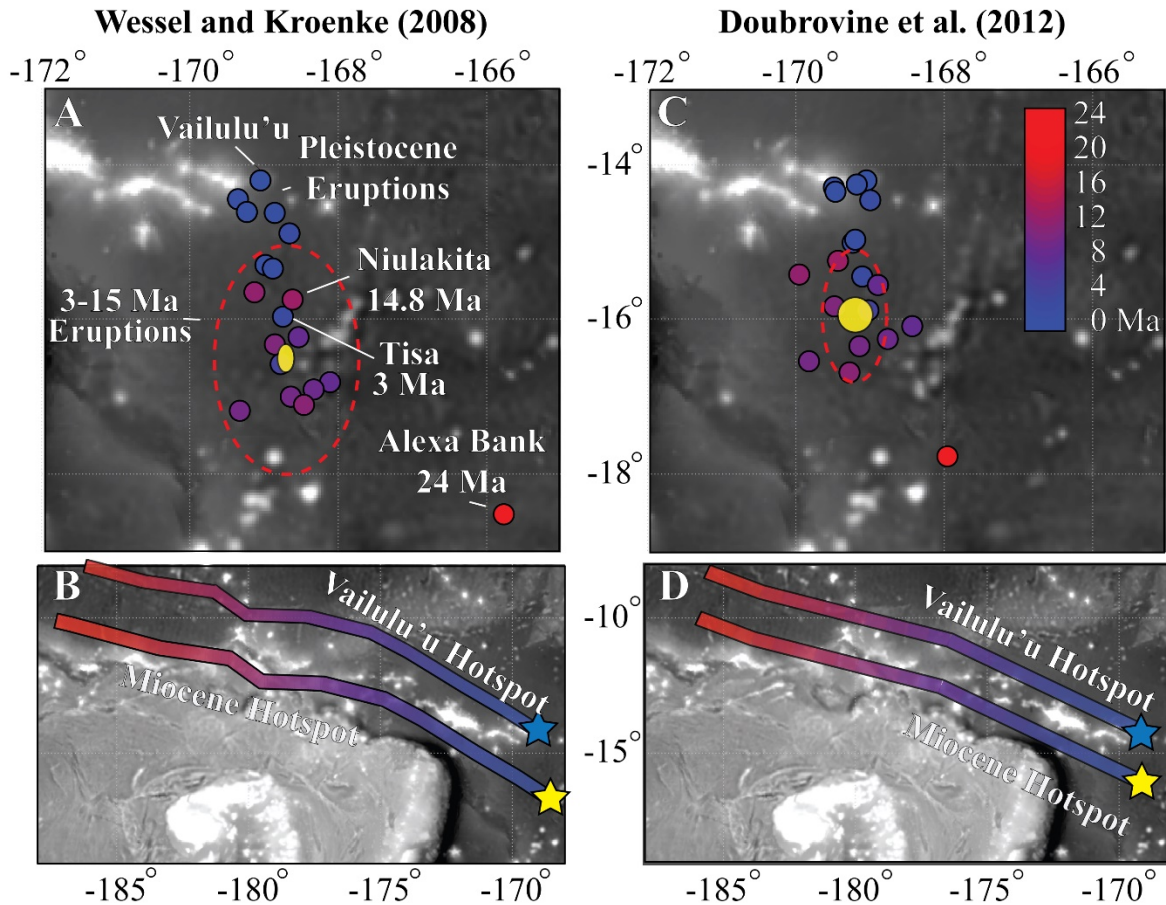


200  
 201 **Figure 1:** A bathymetric map of the Samoan Seamount Province. The seamounts, dredge  
 202 locations (red dots) and oldest  $^{40}\text{Ar}/^{39}\text{Ar}$  age determinations for each feature used in this study are  
 203 shown. The color scaled bar (see **Fig 3** for ages) represents the mean hotspot track path and age  
 204 progression, determined using a piecewise cubic hermite interpolating polynomial of seamount  
 205 locations and calculated age progressions. The mean hotspot track does not match any fixed  
 206 Pacific plate motion model. Bathymetry data is a merged multibeam and satellite altimetry  
 207 dataset from GEBCO ([Weatherall et al., 2015](#)). The white dashed line represents the approximate  
 208 paleo-Vitiaz boundary while the black line shows the region of active subduction.



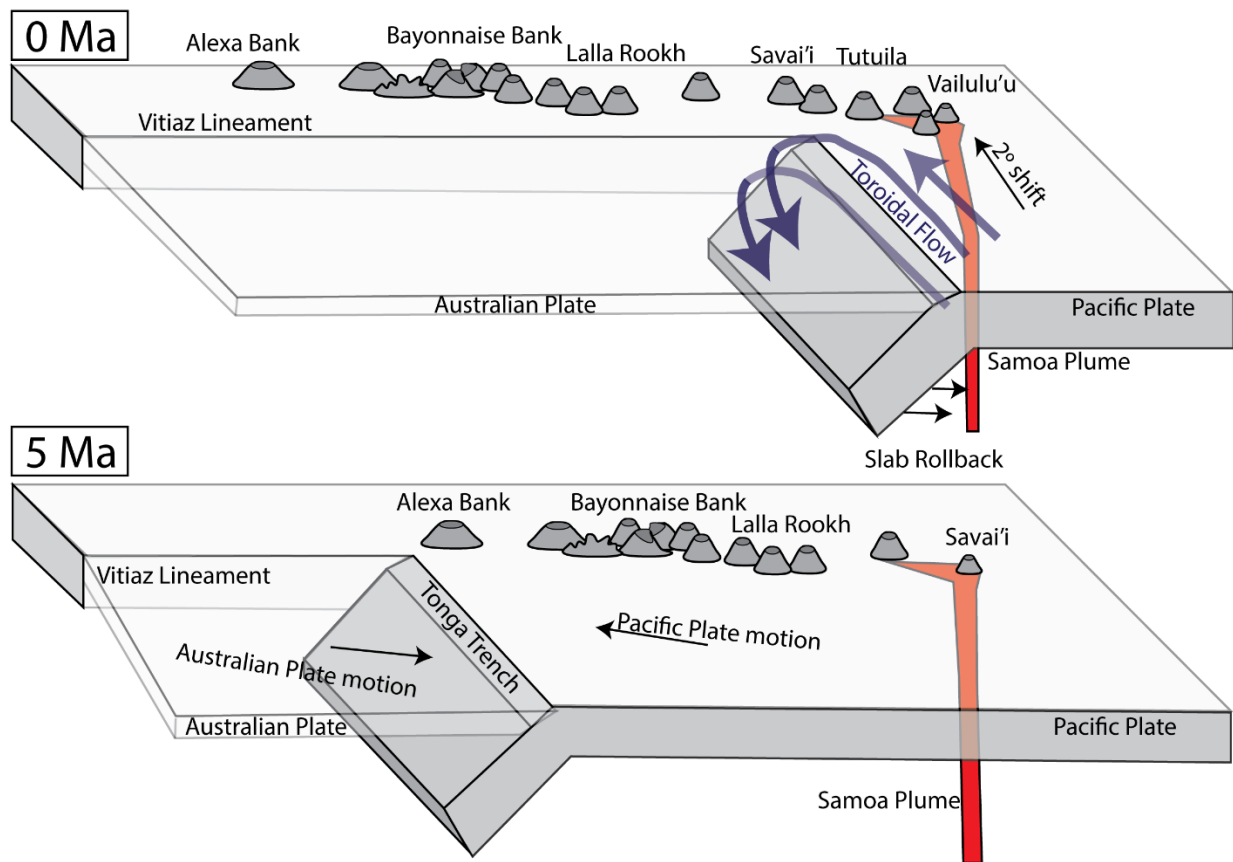
209

210 **Figure 2:** Age versus distance from the hotspot for Samoan lava flow samples in **Table S1**.  
 211 Seamounts are labeled for clarity. The slopes of the lines are indicated and broken into three  
 212 distinct velocity trends. The dotted line represents the mean slope of all the points (0.71°/Ma or  
 213 7.9 cm/a). Included in the calculation is a model age of 9.5 Ma for Lalla Rookh (**Fig. S1**), based  
 214 on the new  $^{40}\text{Ar}/^{39}\text{Ar}$  experimental constraints as well as previous K/Ar age determinations ([Hart](#)  
 215 [et al., 2004](#)). A model age of 9.75 Ma is employed for Sifafi Seamount based on the  $^{40}\text{Ar}/^{39}\text{Ar}$   
 216 incremental heating results (**Fig. S1**).



217

218 **Figure 3:** Absolute plate motion model indicators of plume motion. (A) Reconstructed eruptive  
 219 latitude and longitudes for submarine lava flows with Samoa hotspot-like chemistry using the  
 220 WK08-G fixed hotspot APM model of [Wessel and Kroenke \(2008\)](#). The dots represent the  
 221 reconstructed coordinates with a few key seamounts labeled. The dashed red line represents the  
 222  $2\sigma$  uncertainty ellipse for the 3-15 Ma reconstructed eruptive locations. The yellow ellipse  
 223 represents the modeled mean hotspot location between 3-15 Ma. The size of the yellow ellipse  
 224 represents  $2\sigma$  uncertainties on the mean hotspot location using a Monte Carlo simulation  
 225 ( $n=1000$ ) wherein 40% of the seamounts are randomly excluded each iteration. (B) Modeled  
 226 progressive hotspot tracks using Vailulu'u as the current plume location (blue star) and the  
 227 average 3-15 Ma plume location from 'A' (yellow star). (C) The same as 'A' but using the  
 228 mobile hotspot APM model of [Dobrovine et al. \(2012\)](#). (D) The same as B but with the  
 229 [Dobrovine et al. \(2012\)](#) APM model.



230

231 **Figure 4:** A schematic diagram explaining the observed  $\sim 2^\circ$  N-NW shift of the surface  
 232 expression of the Samoa plume. Shown is the position of the plume at 5 Ma and today. Figure  
 233 influenced by [Price et al. \(2016\)](#). See text for details.

234

235 **REFERENCES**

- 236 Brocher, T.M., 1985. On the formation of the Vitiaz Trench lineament and North Fiji Basin.  
237 Circum-Pacific Council for Energy and Mineral Resources, Earth Science Series,  
238 Houston, Texas.
- 239 Chandler, M.T., Wessel, P., Taylor, B., Seton, M., Kim, S.-S., Hyeong, K., 2012. Reconstructing  
240 Ontong Java Nui: Implications for Pacific absolute plate motion, hotspot drift and true  
241 polar wander. *Earth and Planetary Science Letters* 331, 140-151.
- 242 Doubrovine, P.V., Steinberger, B., Torsvik, T.H., 2012. Absolute plate motions in a reference  
243 frame defined by moving hot spots in the Pacific, Atlantic, and Indian oceans. *Journal of*  
244 *Geophysical Research: Solid Earth* 117.
- 245 Duncan, R.A., 1985. Radiometric ages from volcanic rocks along the New Hebrides-Samoa  
246 lineament. *Investigations of the Northern Melanesian Borderland, Circum-Pacific*  
247 *Council for Energy and Mineral Resources Earth Science Series*, 3, 67–76.
- 248 Duncan, R.A., Clague, D.A., 1985. Pacific plate motion recorded by linear volcanic chains, *The*  
249 *ocean basins and margins Vol.7A: The Pacific Ocean*, Springer, pp. 89-121.
- 250 Finlayson, V., Konter, J., Konrad, K., Koppers, A., Jackson, M., Rooney, T., 2018. Sr–Pb–Nd–  
251 Hf isotopes and <sup>40</sup>Ar/<sup>39</sup>Ar ages reveal a Hawaii–Emperor-style bend in the Rurutu  
252 hotspot. *Earth and Planetary Science Letters* 500, 168-179.
- 253 Gaastra, K.M., Gordon, R.G. and Woodworth, D.T., 2022. Quantification of Pacific Plate  
254 Hotspot Tracks Since 80 Ma. *Tectonics*, 41(7).
- 255 Hart, S.R., Coetzee, M., Workman, R.K., Blusztajn, J., Johnson, K.T.M., Sinton, J.M.,  
256 Steinberger, B., Hawkins, J.W., 2004. Genesis of the Western Samoa seamount province:  
257 age, geochemical fingerprint and tectonics. *Earth and Planetary Science Letters* 227, 37-  
258 56.
- 259 Hart, S.R., Staudigel, H., Koppers, A.A., Blusztajn, J., Baker, E., Workman, R., Jackson, M.,  
260 Hauri, E., Kurz, M., Sims, K., 2000. Vailulu'u undersea volcano: The new Samoa.  
261 *Geochemistry, Geophysics, Geosystems* 1(12).
- 262 Konrad, K., Koppers, A.A., Steinberger, B., Finlayson, V.A., Konter, J.G., Jackson, M.G., 2018.  
263 On the relative motions of long-lived Pacific mantle plumes. *Nature communications* 9,  
264 854.
- 265 Konter, J.G., Finlayson, V.A., Konrad, K., Jackson M.G., Koppers, A.A.P., Wessel, P.,  
266 Alverson, A., Kelley, C. (In revision) The longest-lived Pacific hotspots reveal a plume  
267 tail for the largest oceanic plateau. *Nature*. <https://doi.org/10.31223/X5CQ2T>
- 268 Koppers, A.A., Becker, T.W., Jackson, M.G., Konrad, K., Müller, R.D., Romanowicz, B.,  
269 Steinberger, B., Whittaker, J.M., 2021. Mantle plumes and their role in Earth processes.  
270 *Nature Reviews Earth & Environment* 2, 382-401.
- 271 Koppers, A.A., Russell, J.A., Jackson, M.G., Konter, J., Staudigel, H., Hart, S.R., 2008. Samoa  
272 reinstated as a primary hotspot trail. *Geology* 36, 435-438.
- 273 Koppers, A.A., Russell, J.A., Roberts, J., Jackson, M.G., Konter, J.G., Wright, D.J., Staudigel,  
274 H., Hart, S.R., 2011. Age systematics of two young en echelon Samoan volcanic trails.  
275 *Geochemistry, Geophysics, Geosystems* 12(7).
- 276 Koppers, A.A.P., Yamazaki, T., Geldmacher, J., Gee, J.S., Pressling, N., Hoshi, H., Anderson,  
277 L., Beier, C., Buchs, D.M., Chen, L.H., 2012. Limited latitudinal mantle plume motion  
278 for the Louisville hotspot. *Nature Geoscience* 5, 911-917
- 279 Morgan, W.J., 1972. Deep mantle convection plumes and plate motions. *AAPG Bulletin* 56, 203-  
280 213



281 Price, A.A., Jackson, M.G., Blichert-Toft, J., Blusztajn, J., Conatser, C.S., Konter, J.G., Koppers,  
282 A.A. and Kurz, M.D., 2016. Geochemical evidence in the northeast Lau Basin for  
283 subduction of the Cook-Austral volcanic chain in the Tonga Trench. *Geochemistry,*  
284 *Geophysics, Geosystems*, 17(5), 1694-1724.

285 Price, A.A., Jackson, M.G., Blichert-Toft, J., Konrad, K., Bizimis, M., Koppers, A.A., Konter,  
286 J.G., Finlayson, V.A., Sinton, J.M., 2022. Distinguishing volcanic contributions to the  
287 overlapping Samoan and Cook-Austral hotspot tracks. *Journal of Petrology* 63(5),  
288 p.egac032.

289 Reinhard, A.A., Jackson, M.G., Blusztajn, J., Koppers, A.A., Simms, A.R., Konter, J.G., 2019.  
290 “Petit Spot” Rejuvenated Volcanism Superimposed on Plume-Derived Samoan Shield  
291 Volcanoes: Evidence From a 645-m Drill Core From Tutuila Island, American Samoa.  
292 *Geochemistry, Geophysics, Geosystems*. 20(3), pp.1485-1507.

293 Ruellan, E., Delteil, J., Wright, I. and Matsumoto, T., 2003. From rifting to active spreading in  
294 the Lau Basin–Havre Trough backarc system (SW Pacific): Locking/unlocking induced  
295 by seamount chain subduction. *Geochemistry, Geophysics, Geosystems*, 4(5).

296 Sims, K.W., Hart, S., Reagan, M., Blusztajn, J., Staudigel, H., Sohn, R., Layne, G., Ball, L.,  
297 Andrews, J., 2008.  $^{238}\text{U}$ - $^{230}\text{Th}$ - $^{226}\text{Ra}$ - $^{210}\text{Pb}$ - $^{210}\text{Po}$ ,  $^{232}\text{Th}$ - $^{228}\text{Ra}$ , and  $^{235}\text{U}$ - $^{231}\text{Pa}$   
298 constraints on the ages and petrogenesis of Vailulu'u and Malumalu Lavas, Samoa.  
299 *Geochemistry, Geophysics, Geosystems* 9(4).

300 Sella, G. F., Dixon, T. H., & Mao, A. (2002). REVEL: A model for recent plate velocities from  
301 space geodesy. *Journal of Geophysical Research: Solid Earth*, 107(B4), ETG-11.

302 Steinberger, B., 2000. Plumes in a convecting mantle: Models and observations for individual  
303 hotspots. *Journal of Geophysical Research: Solid Earth* 105, 11127-11152.

304 Strak, V., Schellart, W.P., 2018. A subduction and mantle plume origin for Samoan volcanism.  
305 *Scientific Reports* 8, 10424.

306 Tarduno, J.A., Duncan, R.A., Scholl, D.W., Cottrell, R.D., Steinberger, B., Thordarson, T., Kerr,  
307 B.C., Neal, C.R., Frey, F.A., Torii, M., 2003. The Emperor Seamounts: Southward  
308 motion of the Hawaiian hotspot plume in Earth's mantle. *Science* 301, 1064-1069.

309 Weatherall, P., Marks, K.M., Jakobsson, M., Schmitt, T., Tani, S., Arndt, J.E., Rovere, M.,  
310 Chayes, D., Ferrini, V., Wigley, R., 2015. A new digital bathymetric model of the world's  
311 oceans. *Earth and space Science* 2, 331-345.

312 Wessel, P., Kroenke, L., 1997. A geometric technique for relocating hotspots and refining  
313 absolute plate motions. *Nature* 387, 365-369.

314 Wessel, P., Kroenke, L.W., 2008. Pacific absolute plate motion since 145 Ma: An assessment of  
315 the fixed hot spot hypothesis. *Journal of Geophysical Research: Solid Earth* (1978–2012)  
316 113.

317 Wessel, P., Kroenke, L.W., 2009. Observations of geometry and ages constrain relative motion  
318 of Hawaii and Louisville plumes. *Earth and Planetary Science Letters* 284, 467-472.

319 Workman, R.K., Hart, S.R., Jackson, M., Regelous, M., Farley, K.A., Blusztajn, J., Kurz, M. and  
320 Staudigel, H., 2004. Recycled metasomatized lithosphere as the origin of the Enriched  
321 Mantle II (EM2) end-member: Evidence from the Samoan Volcanic Chain.  
322 *Geochemistry, Geophysics, Geosystems*, 5(4).

1 **Toroidal Flow Around the Tonga Slab Moved the Samoan Plume**  
2 **During the Pliocene**

3  
4 **SUPPLEMENTAL MATERIAL**

5  
6 Kevin Konrad<sup>1\*</sup>; Matthew Jackson<sup>2</sup>; Bernhard Steinberger<sup>3</sup>; Anthony Koppers<sup>4</sup>; Andrea Balbas<sup>5</sup>;  
7 Valerie Finlayson<sup>6</sup>; Jasper Konter<sup>7+</sup>; Allison Price<sup>8</sup>

8  
9 1. Department of Geoscience, University of Nevada Las Vegas, Las Vegas, Nevada 89154, USA

10 2. Department of Earth Science, University of California Santa Barbara, California 93106, USA

11 3. GFZ German Research Centre for Geosciences, Telegrafenberg, 14473 Potsdam, Germany

12 4. College of Earth, Ocean and Atmospheric Sciences, Oregon State University, Corvallis,  
13 Oregon 97331 USA

14 5. Department of Geological Sciences, California State University Long Beach, Long Beach, CA  
15 90840, USA

16 6. Department of Geology, University of Maryland College Park, College Park, Maryland 20742

17 7. Department of Earth Sciences, School of Ocean and Earth Science and Technology,  
18 University of Hawai‘i Mānoa, Honolulu, Hawaii 96822 USA

19 8. Los Alamos National Laboratory, Los Alamos, New Mexico, USA, 87545, USA

20  
21 \*Corresponding author. Phone: (702) 895-3696; Email: Kevin.Konrad@unlv.edu  
22  
23  
24

## 25 New $^{40}\text{Ar}/^{39}\text{Ar}$ Age Determination Methods and Results

26 Recovered dredge samples from expedition RR1310 were chosen for  $^{40}\text{Ar}/^{39}\text{Ar}$  age  
27 determinations based on petrographic analyses. Rocks containing relatively unaltered  
28 phenocrysts (plagioclase, hornblende) or holocrystalline groundmass were chosen for analyses.  
29 All samples were prepared and analyzed using the standard methods described in [Konrad et al.](#)  
30 [\(2018\)](#). Age determinations from the heating experiments were calculated using ArArCalc v2.7.0  
31 [\(Koppers, 2002\)](#). A fluence monitor age of  $28.201 \pm 0.046$  Ma (Kuiper et al., 2008) was used for  
32 the J-curve calibration and a decay rate of  $5.530 \pm 0.097 \times 10^{-10} \text{ yr}^{-1}$  [\(Min et al., 2000\)](#) was used  
33 to calculate the ages. Uncertainties discussed here are  $2\sigma$  internal errors (see [Konrad et al., 2019](#)  
34 for description on how uncertainties are calibrated) with external errors provided on summary  
35 tables in the appendix. Qualifying plateaus required a probability of fit value (P) of  $> 5\%$  with at  
36 least 50% the total  $^{39}\text{Ar}$  released.

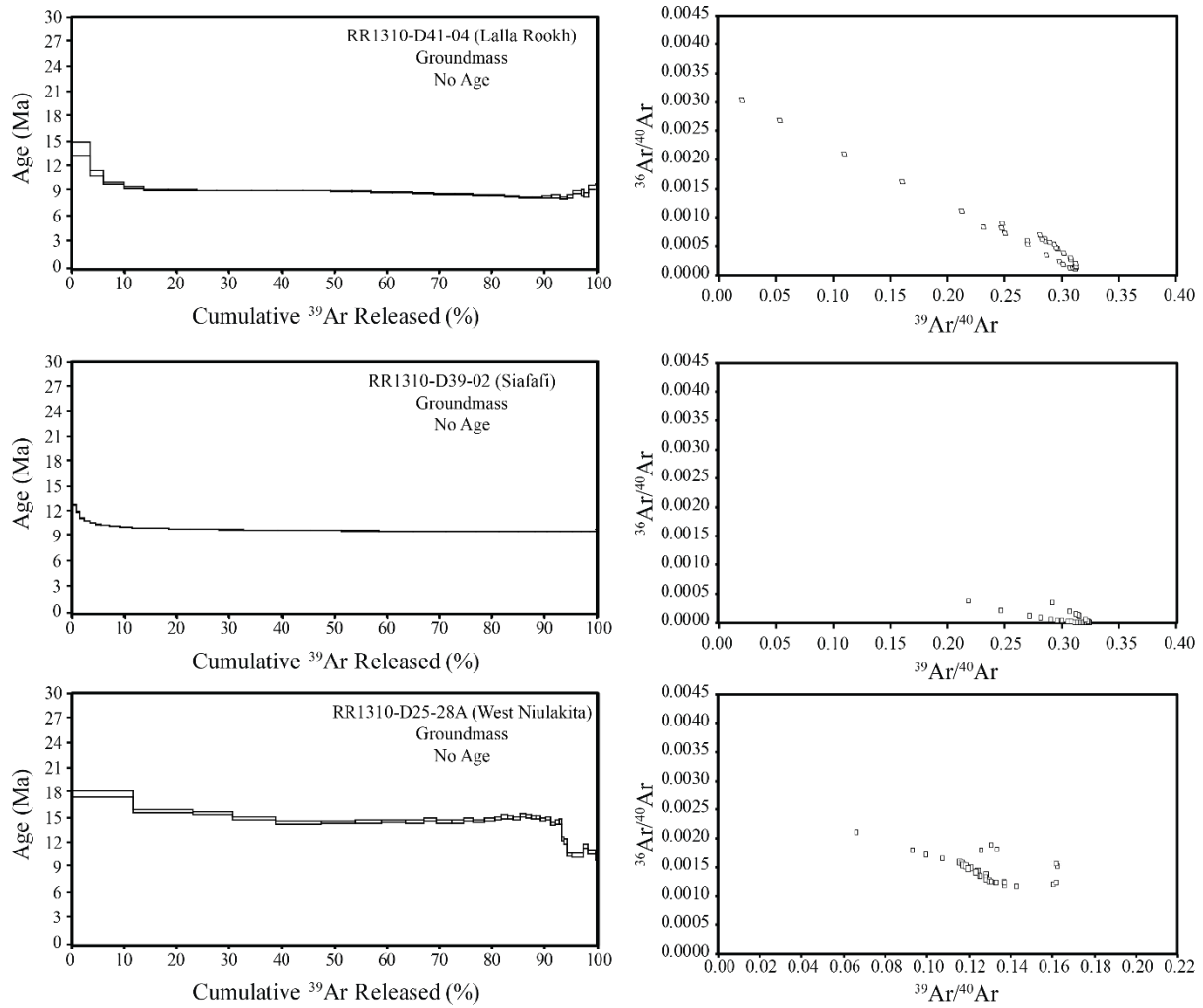
37 A dredge of Siafiifi Seamount (D39) recovered a trachytic lava flow (D39-02). A  
38 groundmass separate of that lava flow contained very high K/Ca (total fusion equivalent = 1.7)  
39 corresponding to individual steps with 0.1% uncertainty levels. The high precision coupled with  
40 a slight continuous recoil pattern (systematically decreasing apparent ages) resulted in a  
41 discordant age spectrum that is not usable by the statistical standards of the  $^{40}\text{Ar}/^{39}\text{Ar}$  community  
42 (e.g. [Schaen et al., 2020](#)). However, despite the consistent recoil pattern the lava flow age is  
43 clearly *ca.* 10 – 9.5 Ma. A groundmass separate from lava flow D41-04, recovered from Lalla  
44 Rookh seamount, produced a discordant heating spectrum. There is a concordant mini-plateau  
45 (31%) that produced an age of *ca.* 9.4 Ma. Similarly, the groundmass separate was attempted  
46 from RR1310-D25-28a (West Niulakita) that did not produce a statistically robust heating  
47 spectrum. The sampled produced a ‘mini-plateau’ (40%  $^{39}\text{Ar}$  released) at *ca.* 14.7 Ma, which is in  
48 line with the younger ages reported from East Niulakita (13.4-14.8; [Finlayson et al., 2018](#)).

## 49 First-order Samoa Plume Motion Calculation

50 The observation of a  $\sim 2^\circ$  northward shift in the surface expression of the Samoan plume  
51 conduit provides an important physical constraint for refining models of mantle flow and plume  
52 migration. Here we provide a first-order assessment of whether the observation is consistent with  
53 previous constraints on plume conduit deflection. If a plume conduit rises through the horizontal  
54 flow of the asthenosphere, the deflection should be the depth integral of horizontal flow divided



55 by rising speed. Plume rising speed in the upper mantle should be of the order 7-10 cm a<sup>-1</sup>  
56 (Steinberger and O'Connell, 2000; Steinberger and Antretter, 2006). Slab rollback in the  
57 northern Tonga trench is about 550 km in 7 Ma (reported by van de Lagemaat et al., 2018), i.e.  
58 about 8 cm a<sup>-1</sup>. Strak and Schellart (2018) observe for similar amounts of rollback flow speeds of  
59 the order 5 cm a<sup>-1</sup>. Assuming channel flow between 100 and 670 km, this would lead to  
60 deflections of:  $570 \text{ km} * 5 \times 10^{-5} \text{ km a}^{-1} * 2 / 3 / 10 \times 10^{-5} \text{ km a}^{-1} = 190 \text{ km} (\sim 1.7^\circ)$  for a rise speed  
61 10 cm a<sup>-1</sup> and 270 km ( $\sim 2.4^\circ$ ) for 7 cm a<sup>-1</sup>, which fits very well with the  $\sim 2^\circ$  northward migration  
62 since the effect of the toroidal flow around the slab edge began (observed in this study).



63  
 64 **Figure S1:**  $^{40}\text{Ar}/^{39}\text{Ar}$  incremental heating results for lava flows from Lalla Rookh, Siafafi and  
 65 West Niulakita. Note that none of the samples produced a statistically concordant plateau or  
 66 isochron age. (Left) Incremental apparent age diagrams as a function of  $^{39}\text{Ar}$  released. (Right)  
 67 The inverse isochron diagrams.  
 68

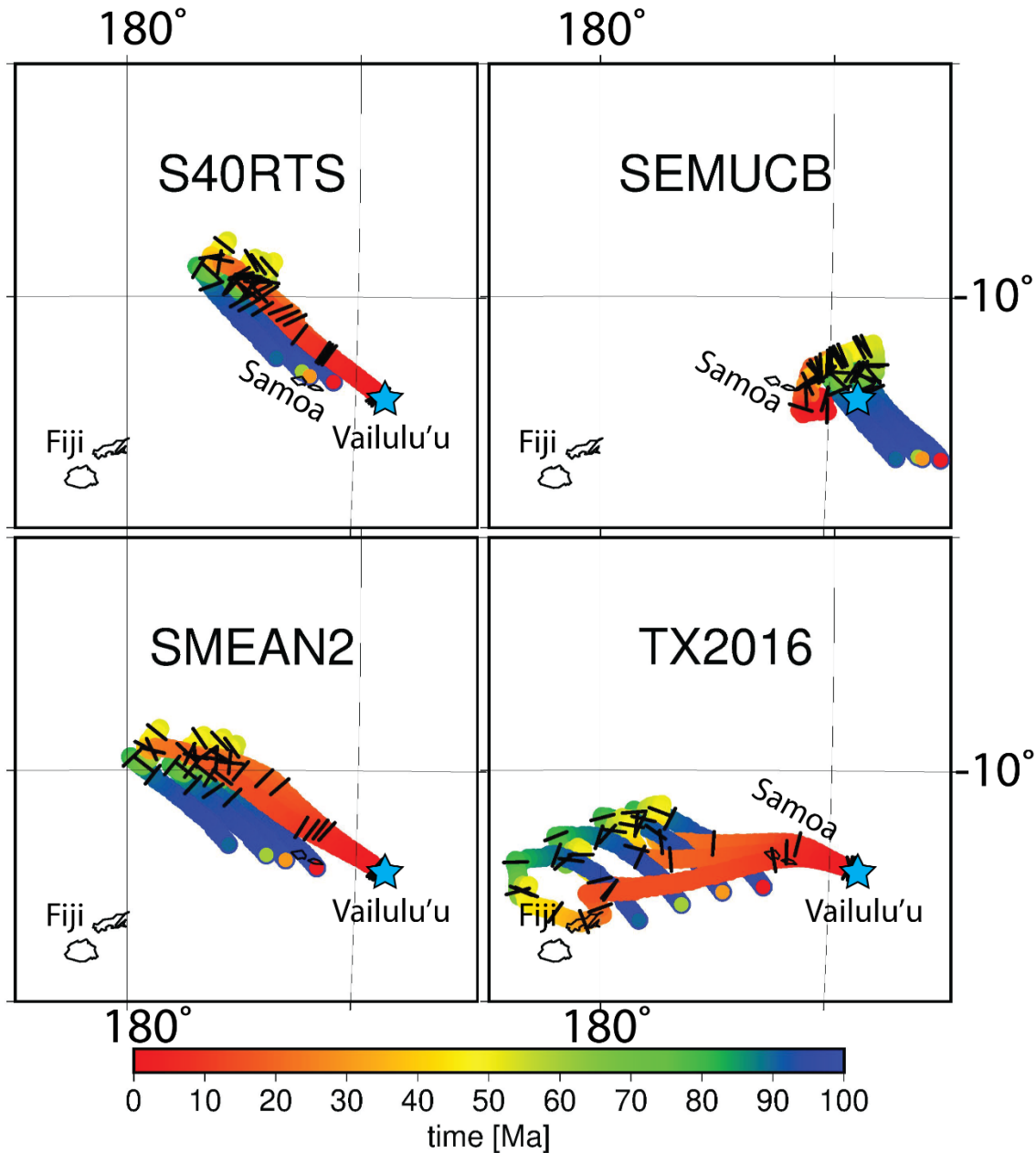
**Table S1: Lava Flows Used in Age Progression Calculations**

Sample	Seamount	Lat	Long	Age (Ma)	2 $\sigma$ (Ma)	Reference
Hotspot	Vailulu'u	-14.20	190.95	0	0	Hart et al., 2000
Alia 103-07	Ofu	-14.102	190.095	0.56	0.07	Koppers et al., 2011
Alia 104-09	Muli	-14.018	189.812	0.97	0.11	Koppers et al., 2011
Alia 109-20	Tulaga	-14.652	189.977	1.06	0.09	Koppers et al., 2011
Alia 110-23	Soso	-13.768	189.758	1.43	0.06	Koppers et al., 2011
Alia 108-04	Tutuila	-14.470	189.700	1.48	0.41	Koppers et al., 2011
Alia 111-05	Tamai'i	-13.755	189.465	2.07	0.06	Koppers et al., 2011
Alia 113-28	Tisa	-14.432	188.668	3.00	0.18	Koppers et al., 2011
Alia 115-18	Savai'i	-14.092	187.058	5.29	0.21	Koppers et al., 2011
RR1310-D41-04	Lalla Rookh	-12.902	184.618	9.50	0	This Paper
RR1310-D39-02	Siafiafi	-12.267	183.942	9.75	0	This Paper
	Waterwitch					
RR1310-D38-41	Bank	-12.778	183.502	10.49	0.09	Price et al. 2022
Alia 123-03	Combe	-12.748	182.632	11.18	0.17	Koppers et al., 2011
RR1310-D32-01	Lafetoga	-12.943	181.962	11.18	0.06	Koppers et al., 2011
RR1310-D33-05	Tuscarora Bank	-12.044	181.541	12.24	0.13	Koppers et al., 2011
Alia 125-04*	Favavesi	-12.696	181.186	13.16	0.16	Finlayson et al., 2018
RR1310-28B-04	Bayonnaise	-11.333	179.875	13.92	0.1	Finlayson et al., 2018
RR1310-D27-42	Niulakita	-11.006	179.790	14.76	0.08	Finlayson et al., 2018
14-19	Alexa	-11.685	175.047	23.96	0.36	Hart et al., 2004

70

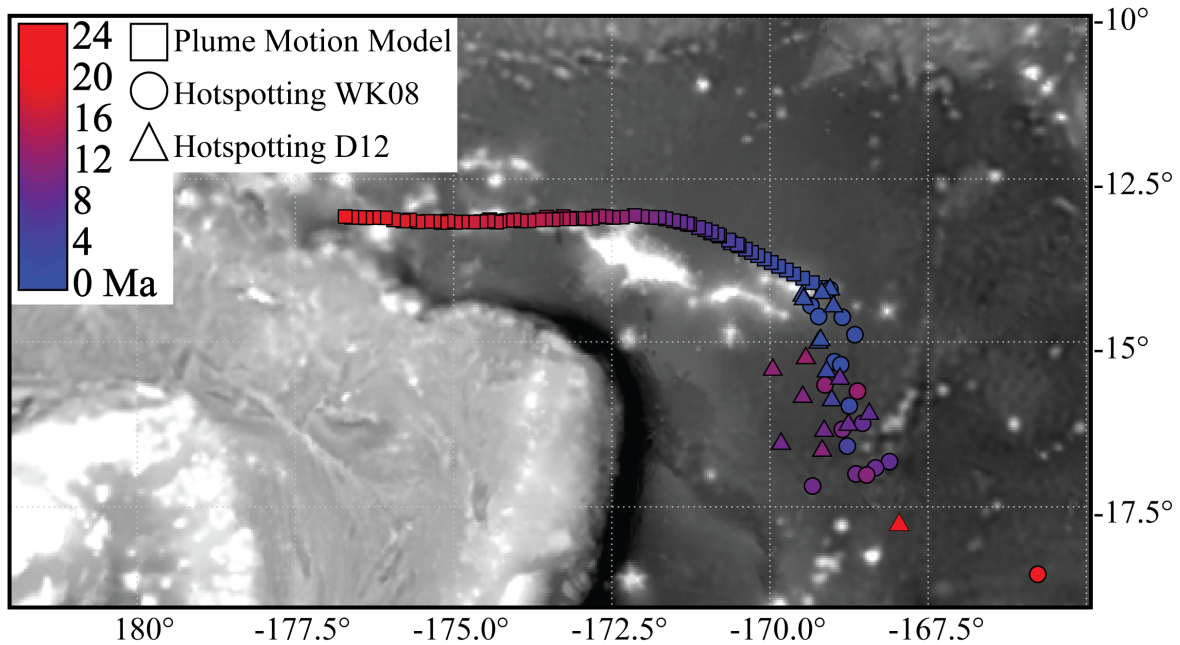
71 *All samples are (re)calculated against a fluence monitor age of  $28.201 \pm 0.046$  Ma (Kuiper et*  
72 *al., 2008) and a decay rate of  $5.530 \pm 0.097 \times 10^{-10} \text{ yr}^{-1}$  (Min et al., 2000). \*The dredge location*  
73 *reported in Koppers et al. (2011) was inaccurate and the location from the cruise report is used*  
74 *here.*

75



76

77 **Figure S2:** Reconstructed surface locations of the Samoan plume using different seismic  
 78 tomography models and plume initiation constraints (e.g. [Steinberger et al. 2019](#)). The color of  
 79 the circles drawn at the initial position where the plume head impacted corresponds to the plume  
 80 head rise time (before that initial time). The age of the plume, when the head impacted, is 100 Ma  
 81 in all cases. The color along the track (from blue=100 Ma to red=0 Ma) corresponds to the time  
 82 when the plume was at that position. Black lines represent 10 Ma intervals. The model uses the  
 83 APM model of [Torsvik et al. \(2010\)](#). S40RTS from [Ritsema et al. \(2011\)](#); SMEAN2 from [Becker  
 84 and Boschi 2002](#); SEMUCB from [French and Romanowicz \(2014\)](#); TX2016 from [Lu and Grand  
 85 \(2016\)](#). Note that the SEMUCB model run failed to ultimately fit the Samoan plume to Vailulu'u  
 86 at time 0.



87  
 88 **Figure S3:** A bathymetric map showing the time-dependent modeled hotspot locations based on  
 89 the eruptive location reconstructions using the APM models of [Wessel and Kroenke \(2008;](#)  
 90 circles), [Dobrovine et al., \(2012;](#) triangles) and a mantle plume motion model using the seismic  
 91 tomography model of TX2016 ([Lu and Grand, 2016](#)) and an instantaneous plume ascent and  
 92 impact age of 100 Ma (bottom right panel in **Fig. S2**). The last 24 Myrs of hotspot locations in  
 93 this model is fairly typically of the results shown in **Fig. S2**.  
 94

95 **References:**

- 96 Becker, T.W. and Boschi, L., 2002. A comparison of tomographic and geodynamic mantle mod-  
97 els. *Geochemistry, Geophysics, Geosystems*, 3(1).
- 98 Doubrovine, P.V., Steinberger, B., Torsvik, T.H., 2012. Absolute plate motions in a reference  
99 frame defined by moving hot spots in the Pacific, Atlantic, and Indian oceans. *Journal of*  
100 *Geophysical Research: Solid Earth* 117.
- 101 Finlayson, V.A., Konter, J.G., Konrad, K., Koppers, A.A.P., Jackson, M.G. and Rooney, T.O.,  
102 2018. Sr–Pb–Nd–Hf isotopes and  $^{40}\text{Ar}/^{39}\text{Ar}$  ages reveal a Hawaii–Emperor-style bend  
103 in the Rurutu hotspot. *Earth and Planetary Science Letters*, 500, pp.168-179.
- 104 French, S.W. and Romanowicz, B.A., 2014. Whole-mantle radially anisotropic shear velocity  
105 structure from spectral-element waveform tomography. *Geophysical Journal Interna-*  
106 *tional*, 199(3), pp.1303-1327.
- 107 Hart, S.R., Staudigel, H., Koppers, A.A., Blusztajn, J., Baker, E.T., Workman, R., Jackson, M.,  
108 Hauri, E., Kurz, M., Sims, K. and Fornari, D., 2000. Vailulu'u undersea volcano: The  
109 new Samoa. *Geochemistry, Geophysics, Geosystems*, 1(12).
- 110 Hart, S.R., Coetzee, M., Workman, R.K., Blusztajn, J., Johnson, K.T.M., Sinton, J.M., Stein-  
111 berger, B. and Hawkins, J.W., 2004. Genesis of the Western Samoa seamount province:  
112 age, geochemical fingerprint and tectonics. *Earth and Planetary Science Letters*, 227(1-  
113 2), pp.37-56.
- 114 Konrad, K., Koppers, A.A., Steinberger, B., Finlayson, V.A., Konter, J.G. and Jackson, M.G.,  
115 2018. On the relative motions of long-lived Pacific mantle plumes. *Nature Communica-*  
116 *tions*, 9(1), p.854.
- 117 Konrad, K., Koppers, A.A., Balbas, A.M., Miggins, D.P. and Heaton, D.E., 2019. Dating  
118 clinopyroxene phenocrysts in submarine basalts using  $^{40}\text{Ar}/^{39}\text{Ar}$  geochronology. *Geo-*  
119 *chemistry, Geophysics, Geosystems*, 20(2), pp.1041-1053.
- 120 Koppers, A.A., 2002. ArArCALC—software for  $^{40}\text{Ar}/^{39}\text{Ar}$  age calculations. *Computers &*  
121 *Geosciences*, 28(5), pp.605-619.
- 122 Koppers, A.A., Russell, J.A., Roberts, J., Jackson, M.G., Konter, J.G., Wright, D.J., Staudigel, H.  
123 and Hart, S.R., 2011. Age systematics of two young en echelon Samoan volcanic trails.  
124 *Geochemistry, Geophysics, Geosystems*, 12(7).
- 125 Kuiper, K.F., Deino, A., Hilgen, F.J., Krijgsman, W., Renne, P.R. and Wijbrans, A.J., 2008. Syn-  
126 chronizing rock clocks of Earth history. *science*, 320(5875), pp.500-504.
- 127 van de Lagemaat, S.H., Van Hinsbergen, D.J., Boschman, L.M., Kamp, P.J. and Spakman, W.,  
128 2018. Southwest Pacific absolute plate kinematic reconstruction reveals major Cenozoic  
129 Tonga-Kermadec slab dragging. *Tectonics*, 37(8), pp.2647-2674.
- 130 Lu, C. and Grand, S.P., 2016. The effect of subducting slabs in global shear wave tomography.  
131 *Geophysical Journal International*, 205(2), pp.1074-1085.
- 132 Min, K., Mundil, R., Renne, P.R. and Ludwig, K.R., 2000. A test for systematic errors in  $^{40}\text{Ar}/$   
133  $^{39}\text{Ar}$  geochronology through comparison with U/Pb analysis of a 1.1-Ga rhyolite.  
134 *Geochimica et Cosmochimica Acta*, 64(1), pp.73-98.
- 135 Price, A.A., Jackson, M.G., Blichert-Toft, J., Konrad, K., Bizimis, M., Koppers, A.A., Konter,  
136 J.G., Finlayson, V.A. and Sinton, J.M., 2022. Distinguishing volcanic contributions to the  
137 overlapping Samoan and Cook-Austral hotspot tracks. *Journal of Petrology*, 63(5), p.e-  
138 gac032.
- 139 Ritsema, J., Deuss, A., Van Heijst, H.J. and Woodhouse, J.H., 2011. S40RTS: a degree-40 shear-  
140 velocity model for the mantle from new Rayleigh wave dispersion, teleseismic traveltimes

141 and normal-mode splitting function measurements. *Geophysical Journal International*,  
142 184(3), pp.1223-1236.

143 Schaen, A.J., Jicha, B.R., Hodges, K.V., Vermeesch, P., Stelten, M.E., Mercer, C.M., Phillips,  
144 D., Rivera, T.A., Jourdan, F., Matchan, E.L. and Hemming, S.R., 2021. Interpreting and  
145 reporting 40Ar/39Ar geochronologic data. *Bulletin*, 133(3-4), pp.461-487.

146 Steinberger, B. and O'Connell, R.J., 2000. Effects of mantle flow on hotspot motion. Washington  
147 DC American Geophysical Union Geophysical Monograph Series, 121, pp.377-398.

148 Steinberger, B. and Antretter, M., 2006. Conduit diameter and buoyant rising speed of mantle  
149 plumes: Implications for the motion of hot spots and shape of plume conduits. *Geochem-*  
150 *istry, Geophysics, Geosystems*, 7(11).

151 Steinberger, B., Nelson, P.L., Grand, S.P. and Wang, W., 2019. Yellowstone plume conduit tilt  
152 caused by large-scale mantle flow. *Geochemistry, Geophysics, Geosystems*, 20(12),  
153 pp.5896-5912.

154 Strak, V. and Schellart, W.P., 2018. A subduction and mantle plume origin for Samoan volcan-  
155 ism. *Scientific Reports*, 8(1), p.10424.

156 Torsvik, T.H., Steinberger, B., Gurnis, M. and Gaina, C., 2010. Plate tectonics and net litho-  
157 sphere rotation over the past 150 My. *Earth and Planetary Science Letters*, 291(1-4),  
158 pp.106-112.

159 Wessel, P., Kroenke, L.W., 2008. Pacific absolute plate motion since 145 Ma: An assessment of  
160 the fixed hot spot hypothesis. *Journal of Geophysical Research: Solid Earth (1978–2012)*  
161 113.